Rarefaction and compressibility effects of the lattice-Boltzmann-equation method in a gas microchannel

Taehun Lee and Ching-Long Lin*
Department of Mechanical and Industrial Engineering, IIHR - Hydroscience & Engineering, The University of Iowa, Iowa City, Iowa 52242, USA
(Received 20 April 2004; revised manuscript received 27 January 2005; published 20 April 2005)

A wall equilibrium boundary condition for an implicit lattice-Boltzmann-equation method is proposed to simulate gas flows in a microchannel with rough surface on the characteristic length of gas molecules. The boundary condition is based on the assumption that impinging molecules reach equilibrium with the surface. The molecular mean free path used to define the Knudsen number is determined by the lattice speed and the relaxation time of the lattice-Boltzmann equation. With the wall equilibrium boundary condition and the appropriate relation defined for the Knudsen number and the relaxation time, the computed slip velocity and nonlinear pressure distribution along the microchannel are in excellent agreement with analytical solutions.

DOI: 10.1103/PhysRevE.71.046706 PACS number(s): 47.11.+j, 02.70.−c, 47.10.+g

I. INTRODUCTION

The slip velocity of the lattice-Boltzmann-equation (LBE) method has been observed since its advent. In the simulation of macroscopic fluid flows, the slip velocity of the LBE method was considered a numerical error that must be corrected. In this regard, efforts have been made for development of the perfect no-slip boundary condition. The bounce-back rule and the equilibrium boundary condition commonly adopted in LBE simulations produce a first-order slip velocity. Even the higher-order boundary conditions that have been proposed during the last decade are not entirely free from the slip velocity [1]. Generally, the slip velocity increases with the relaxation time of intermolecular collision to local equilibrium. At the molecular level, the relaxation time can be related to the Knudsen number Kn, which is the ratio of the lattice molecular mean free path l to the characteristic dimension H. Continuum can be realized only in the zero-Kn limit, while the gas exhibits noncontinuum behaviors such as rarefaction and compressibility effects as Kn increases. The slip velocity of the LBE method can be attributed to the nonzero-Knudsen-number effect. Since the relaxation time is linearly proportional to Kn as will be shown later, the zero-Kn limit, viz., zero relaxation time, is a numerically impossible condition. Nonzero relaxation time implies that the rarefaction effect is always present to a certain degree in the LBE simulation, which is the origin of slip velocity. For a general description of the LBE method and its historical links with statistical mechanics, readers are referred to Benzi *et al.* [2] and Chen and Doolen [3].

As the characteristic length scale of the system approaches the mean free path, the continuum hypothesis starts to break down and so does the no-slip condition, which is just an empirical finding in the continuum regime. On this small length scale, the slip velocity due to rarefaction attains physical grounds, since it originates from the kinetic nature and mesoscopic dynamics of the LBE method, and thus the LBE method can be a promising tool for simulation of gas flows on the microscale. Conducting experiments in micrometer-size geometries is a big challenge [4,5] and the direct simulation Monte Carlo (DSMC) method [6] usually requires a tremendous amount of computer time and memory. The Navier-Stokes simulation can be utilized in the slip flow regime ($0.01<\mathrm{Kn}<0.1$), but it must be supplemented by some slip velocity boundary conditions [7]. The underlying premise of the slip boundary condition is that flows away from solid boundaries can still be treated as a continuum. However, the slip boundary condition no longer holds in the transition flow regime ($0.1<\mathrm{Kn}<3$), where the continuum assumption breaks down even away from solid boundaries.

Recently, Nie *et al.* [8] applied the LBE method to simulation of microflows in a channel and cavity. They used the explicit LBE formulation [9] and related the nondimensional relaxation time τ_e to Kn as $\mathrm{Kn}=\alpha(\tau_e-0.5)/\rho H$ for a microchannel of height H and gas density ρ. The factor 0.5 comes from the explicit treatment of the collision term and α is chosen to best match the simulated mass flow rate with experiments. Nie *et al.* [8] used the halfway bounce-back rule for the slip effect at the surface. Later, Lim *et al.* [10] proposed a different relation between Kn and τ_e for the explicit LBE formulation and performed a series of simulations of microchannel flows with two different boundary conditions. Their Kn for a long microchannel was defined as $\mathrm{Kn}=(\delta x\tau_e/H)(P_o/P)$, where P and P_o are the local pressure and the pressure at the outlet of the channel, respectively. Their nondimensional relaxation time τ_e, however, did not include the correction factor of 0.5 as in Nie *et al.* [8]. The specular bounce-back rule and the extrapolation scheme were employed to generate the slip effect. Both boundary conditions yielded qualitatively similar results.

Although previous LBE simulations show promising results to some extent, their conclusions do not converge. The definition of Kn is still not in consensus. Different boundary conditions such as the typical bounce-back rule, the specular bounce-back rule, and the extrapolation scheme are used to generate the slip effect and even in some cases, the no-slip

*Electronic address: ching-long-lin@uiowa.edu

effect. For instance, the bounce-back rule was used for the slip effect by Nie *et al.* [8], while it was considered as a no-slip boundary condition by Succi [11]. Generally, the bounce-back rule is known to satisfy the macroscopic no-slip boundary condition only up to first-order accuracy. The slip error induced by the bounce-back rule seems to increase with the relaxation time [12] and is hardly distinguishable from the physical the slip effect. To produce the slip effect, Succi introduced the specular bounce-back rule and studied velocity slip. Furthermore, most of the simulations were carried out on very coarse grids, e.g., $H=10\delta x$ by Nie *et al.* [8] (δx is the grid spacing) and $H=10\delta x \sim 20\delta x$ with fixed $L/H=10$ (L is the channel length) by Lim *et al.* [10]. Fine grid calculation has not been reported to our knowledge.

The objective of this paper is to propose a dimensionally consistent definition of Kn and a boundary condition which generate velocity slip in a physically meaningful manner. We assume that gas molecules travel the distance of the lattice mean free path l with the lattice speed $c=\delta x/\delta t$ while relaxing to their equilibrium state in the relaxation time λ. The definition of Kn is then similar to that of Lim *et al.*, but consistent, implicit discretization of the discrete Boltzmann equation (DBE) indicates that the second-order accurate τ-Kn relation requires a correction factor of 0.5 to the τ-Kn relation proposed by Lim *et al.* [10]. As to the boundary condition, we assume that the impinging molecules represented by the particle distribution functions reach equilibrium with the surface. Since the surface is rough on the characteristic length scale of gas molecules, the reflection of the molecules is diffuse and the equilibrium state at the surface can be justified. In fact, Ansumali and Karlin [13] recently proposed a diffusive boundary condition to ensure the positivity of the reflected distribution functions and the condition of detailed balance. They showed that with proper implementation of the boundary condition, the solution of the LBE method converges to the hydrodynamic limit in the same way as the Boltzmann equation.

To confirm the relationship between the slip velocity and Kn, we first consider periodic microchannel flows driven by a constant external pressure gradient. Although the compressibility effect is absent in the periodic channel flows involved, the computed slip velocity can be treated as a slip velocity at the outlet in a very long microchannel. We carry out a series of computations that vary the number of grid points in a systematic way ($H=10\delta x-320\delta x$) and prove the second-order accuracy of the relationship between the slip velocity and Kn. Then, we examine both the rarefaction and compressibility effects in a long microchannel with pressure boundary conditions at the inlet and outlet. We compare the normalized slip velocity and pressure nonlinearity along the channel with the analytical formula derived by Arkilic *et al.* [14] and the numerical results of Lim *et al.* [10]. Unlike previous LBE results [8,10], which show significant deviation from the analytical formula of Arkilic *et al.*, our results are generally in excellent agreement with the analytical formula. The disagreement of the previous results can be ascribed to the improper τ-Kn relations and boundary conditions. Lack of fine grid calculations could be another reason.

The paper is organized as follows. In Sec. II, a formulation of the LBE with external forcing terms is presented. In Sec. III, the Knudsen number and its relation to the relaxation time are defined in the framework of the LBE. A wall equilibrium boundary condition is then discussed and compared with previously proposed boundary conditions. Section IV is devoted to the rarefaction and compressibility effects of the present LBE method. Concluding remarks are given in Sec. V.

II. LATTICE-BOLTZMANN EQUATION

A DBE with an external forcing term F_i is proposed by He *et al.* [15] and can be written as

$$\frac{\partial f_\alpha}{\partial t}+e_{\alpha i}\frac{\partial f_\alpha}{\partial x_i}=-\frac{f_\alpha-f_\alpha^{\mathrm{eq}}}{\lambda}+\frac{(e_{\alpha i}-u_i)F_i}{c_s^2\rho}f_\alpha^{\mathrm{eq}}, \tag{2.1}$$

where f_α is the particle distribution function, $e_{\alpha i}$ is the microscopic particle velocity, u_i is the macroscopic velocity, c_s is the speed of sound, and λ is the relaxation time, whose inverse is also known as the collision frequency of the particles [16]. The equilibrium distribution function f_α^{eq} is given by

$$f_\alpha^{\mathrm{eq}}=t_\alpha\rho\left[1+\frac{e_{\alpha i}u_i}{c_s^2}+\frac{(e_{\alpha i}e_{\alpha j}-c_s^2\delta_{ij})u_iu_j}{2c_s^4}\right]. \tag{2.2}$$

t_α is a weighting factor and ρ is the density. In a nine-velocity LBE model on a square lattice, the discrete velocity $\mathbf{e}_\alpha$ is expressed as

$$\mathbf{e}_\alpha=\begin{pmatrix} c(0,0) & & \alpha=0 \\ c(\cos\theta_\alpha,\sin\theta_\alpha) & \theta_\alpha=(\alpha-1)\pi/4 & \alpha=1,3,5,7 \\ \sqrt{2}c(\cos\theta_\alpha,\sin\theta_\alpha) & \theta_\alpha=(\alpha-1)\pi/4 & \alpha=2,4,6,8 \end{pmatrix}, \tag{2.3}$$

in which the speed of sound c_s is related to the lattice molecular speed c by $c_s=c/\sqrt{3}$. For this specific model, the weighting factors are given as $t_0=4/9$, $t_1=t_3=t_5=t_7=1/9$, and $t_2=t_4=t_6=t_8=1/36$ [17]. The external forcing term F_i can represent a constant pressure gradient in a periodic channel. In the present study, a nine-velocity LBE model on a square lattice is used.

The LBE for f_α is obtained by discretizing Eq. (2.1) along characteristics over the time step δt [9]:

$$f_\alpha(\mathbf{x}+\mathbf{e}_\alpha\delta t,t+\delta t)-f_\alpha(\mathbf{x},t)=-\int_t^{t+\delta t}\frac{f_\alpha-f_\alpha^{\mathrm{eq}}}{\lambda}dt'+\int_t^{t+\delta t}\frac{(e_{\alpha i}-u_i)F_i}{c_s^2\rho}f_\alpha^{\mathrm{eq}}dt'. \tag{2.4}$$

Note that the time integration in $[t,t+\delta t]$ is coupled with the space integration in $[\mathbf{x},\mathbf{x}+\mathbf{e}_\alpha\delta t]$. Application of the trapezoidal rule for second-order accuracy and unconditional stability leads to

$$f_\alpha(\mathbf{x}+\mathbf{e}_\alpha\delta t, t+\delta t) - f_\alpha(\mathbf{x},t) = -\left.\frac{f_\alpha - f_\alpha^{\mathrm{eq}}}{2\tau}\right|_{(\mathbf{x},t)} - \left.\frac{f_\alpha - f_\alpha^{\mathrm{eq}}}{2\tau}\right|_{(\mathbf{x}+\mathbf{e}_\alpha\delta t, t+\delta t)} + \frac{\delta t}{2}\left.\frac{(e_{\alpha i}-u_i)F_i}{c_s^2\rho} f_\alpha^{\mathrm{eq}}\right|_{(\mathbf{x},t)} + \frac{\delta t}{2}\left.\frac{(e_{\alpha i}-u_i)F_i}{c_s^2\rho} f_\alpha^{\mathrm{eq}}\right|_{(\mathbf{x}+\mathbf{e}_\alpha\delta t, t+\delta t)}, \tag{2.5}$$

where the nondimensional relaxation time $\tau = \lambda/\delta t$.

Here, we introduce a modified particle distribution function $\overline{f}_\alpha$ to facilitate computation:

$$\overline{f}_\alpha = f_\alpha + \frac{f_\alpha - f_\alpha^{\mathrm{eq}}}{2\tau} - \frac{\delta t}{2}\frac{(e_{\alpha i}-u_i)F_i}{c_s^2\rho} f_\alpha^{\mathrm{eq}}. \tag{2.6}$$

The above LBE can then be recast in a simpler form [18]:

$$\overline{f}_\alpha(\mathbf{x}+\mathbf{e}_\alpha\delta t, t+\delta t) - \overline{f}_\alpha(\mathbf{x},t) = -\left.\frac{1}{\tau+0.5}(\overline{f}_\alpha - f_\alpha^{\mathrm{eq}})\right|_{(\mathbf{x},t)} + \frac{\tau\delta t}{\tau+0.5}\left.\frac{(e_{\alpha i}-u_i)F_i}{c_s^2\rho} f_\alpha^{\mathrm{eq}}\right|_{(\mathbf{x},t)}, \tag{2.7}$$

which can be solved in two steps: the collision step

$$\overline{f}_\alpha(\mathbf{x},t) = \overline{f}_\alpha(\mathbf{x},t) - \left.\frac{1}{\tau+0.5}(\overline{f}_\alpha - f_\alpha^{\mathrm{eq}})\right|_{(\mathbf{x},t)} + \frac{\tau\delta t}{\tau+0.5}\left.\frac{(e_{\alpha i}-u_i)F_i}{c_s^2\rho} f_\alpha^{\mathrm{eq}}\right|_{(\mathbf{x},t)}, \tag{2.8}$$

and the streaming step

$$\overline{f}_\alpha(\mathbf{x}+\mathbf{e}_\alpha\delta t, t+\delta t) = \overline{f}_\alpha(\mathbf{x},t). \tag{2.9}$$

The density and the velocities are calculated after the streaming step by taking the zeroth and first moments of $\overline{f}_\alpha$,

$$\rho = \sum_\alpha \overline{f}_\alpha, \tag{2.10}$$

$$\rho\mathbf{u} = \sum_\alpha \mathbf{e}_\alpha \overline{f}_\alpha + \frac{\delta t}{2}\mathbf{F}, \tag{2.11}$$

and the pressure is computed by the ideal gas equation of state $P = c_s^2\rho$.

Recall that the above LBE is fully implicit for the relaxation term and the forcing term alike and therefore is unconditionally stable. When τ approaches zero, the amplification factor of the collision step turns negative and solutions tend to be oscillatory as a result [9].

III. KNUDSEN NUMBER AND BOUNDARY CONDITION

For the continuum flow the relaxation time is given as $\lambda = \nu/c_s^2$ in which ν is the kinematic viscosity, while for the microflow the relaxation time can be related to Kn as well. The mean free path l is defined by the ratio of the lattice molecular speed $c = \delta x/\delta t$ to the collision frequency of the particles $1/\lambda$ [19]:

$$l = c\lambda. \tag{3.1}$$

Typically, λ is a time scale associated with collisional relaxation to the local equilibrium, which enables us to relate λ to l. Here we use the word "molecular" as a general term to mean pseudomolecules as understood in particle methods. The assumption leads to the definition of Kn as by Inamuro *et al.* [16]:

$$\mathrm{Kn} = \frac{l}{H} = \frac{c\lambda}{H}, \tag{3.2}$$

where H is the channel height in our simulation. Equation (3.2) can be rewritten in terms of the nondimensional relaxation time τ and nondimensional lattice spacing $\delta x/H$,

$$\mathrm{Kn} = \frac{c\lambda}{H} = \frac{\delta x}{\delta t}\frac{\delta t\tau}{H} = \frac{\delta x\tau}{H}. \tag{3.3}$$

It is evident that Kn is related to both τ and $\delta x/H$.

From Eq. (3.3), the viscosity μ of the fluid is given as follows:

$$\frac{\mu}{\rho cH} = \frac{\mathrm{Kn}}{3}. \tag{3.4}$$

Given Eqs. (3.3) and (3.4), Kn defined in the LBE framework can recover the typical macroscopic relation of Kn with the Mach and Reynolds numbers:

$$\mathrm{Kn} \propto \frac{\mathrm{Ma}}{\mathrm{Re}}. \tag{3.5}$$

Hence, Kn increases as Re decreases or Ma increases. In the case of small Re either the fluid density ρ or the channel height H is small, whereas in the case of large Ma flow becomes hypersonic. LBE simulation is valid only for the former case; thus Ma must be kept small for accuracy.

It is noteworthy that τ in Eq. (3.3) is different from that of Lim *et al.* by a factor of 0.5 because the LBE in Eq. (2.7) is derived by using the trapezoidal rule rather than the explicit Euler method. Specifically, the Kn of Lim *et al.* can be expressed by

$$\mathrm{Kn} = \frac{\delta x\tau_e}{H} = \frac{\delta x(\tau+0.5)}{H}, \tag{3.6}$$

which is only first-order accurate. In a long channel the local Knudsen number needs to be modified, since the mean free path is inversely proportional to the pressure,

$$\mathrm{Kn} = \mathrm{Kn}_o \frac{P_o}{P(x,y)} \tag{3.7}$$

where Kn_o and P_o are the Kn and the pressure at the outlet, respectively. The local nondimensional relaxation time τ is determined by the local Kn.

The tangential momentum accommodation coefficient σ_v is a parameter that measures the degree of equilibrium of impinging molecules with the surface [20]. Thus, σ_v is the fraction of diffusely reflected molecules whose average tangential velocity is zero. If the surface is rough on the characteristic length scale of gas molecules, the reflection of the molecules will be diffuse and σ_v approaches unity. Since σ_v of most engineering surfaces is close to unity (for instance, air or CO_2 on machined brass or shellac has $\sigma_v=1$ and air on glass has $\sigma_v=0.89$ [21]), the molecules "forget the past" [22] and reemit after the wall collision with the equilibrium distribution function. At stationary walls, the equilibrium distribution Eq. (2.2) reduces to diffuse reflection, i.e., $f_\alpha^{\mathrm{eq}}=t_\alpha\rho$. The condition for the use of the equilibrium distribution function as a boundary condition of the LBE method is that we have perfect accommodation. Under controlled test conditions, however, the σ_v value could be less than unity [14]. In this case, we may apply a mix of the wall equilibrium boundary condition and the specular reflection in a similar manner to that proposed by Succi [11]. Succi adopted a mix of the bounce-back and specular reflection to incorporate nonunity accommodation effects.

We calculate the equilibrium distribution function using the surface velocity and the density that is obtained by taking the zeroth moment of the particle distribution function after the streaming step with the notion that the impinging particles are simply bounced back. The equilibrium distribution function is then assigned to the particle distribution function at the surface, i.e., $f_\alpha=f_\alpha^{\mathrm{eq}}$. At the inlet and outlet boundary nodes, the second-order extrapolation scheme [23] is utilized to calculate unknown particle distribution functions. The velocity can then be computed by taking the first moment of these functions. Implementation of density (or pressure) boundary condition is not as straightforward as for continuum incompressible flows. This is because in a long microchannel, not only is the pressure distribution along the channel nonlinear but the pressure slightly varies across the channel due to the existence of the vertical velocity component in two-dimensional geometry. Consequently, the prescription of constant density at inlet and outlet boundary nodes distorts flow fields near the inlet and outlet boundaries. In order to prevent this unwanted distortion, we approximate the density at the inlet and outlet boundary nodes by second-order extrapolation from the interior nodes. The extrapolated density is then rescaled to the prescribed density such that the average density across the inlet and outlet boundary nodes remains the prescribed density, while local density variation is allowed along the inlet and outlet boundary nodes.

IV. NUMERICAL EXPERIMENTS

We compare the computed normalized slip velocity with the analytical results of Arkilic *et al.* for a long microchannel. In their analysis, Arkilic *et al.* assumed that the pressure is constant across the channel, the vertical velocity is zero everywhere, and the effect of the inertial term is negligible. The slip velocity normalized to the centerline velocity at the outlet (U_o) can be obtained with the aid of the first-order slip boundary condition (see Appendix A)

$$\frac{U_s(x)}{U_o} = \frac{dP/dx}{dP_o/dx}\frac{\sigma\mathrm{Kn}}{(0.25+\sigma\mathrm{Kn}_o)}, \tag{4.1}$$

where σ represents the streamwise momentum accommodation,

$$\sigma = \frac{2-\sigma_v}{\sigma_v}. \tag{4.2}$$

Then, the normalized slip velocity at the outlet is only dependent on Kn_o at the outlet:

$$\frac{U_{s,o}}{U_o} = \frac{\sigma\mathrm{Kn}_o}{(0.25+\sigma\mathrm{Kn}_o)}. \tag{4.3}$$

Historically, $\sigma_v=1$ has been used for almost all engineering calculations [14]; therefore we take $\sigma_v=1$ throughout the paper. Also note that the analytic results of Arkilic *et al.* used as reference solutions in the following sections are obtained for $\sigma_v=1$. Use of this value is consistent with the applied wall equilibrium boundary condition.

A. Gas flows in a periodic microchannel

To begin with, we study gas flows in a periodic microchannel driven by a constant external pressure gradient in order to validate the second-order spatial accuracy of the wall equilibrium boundary condition and the τ-Kn relation. The periodic boundary condition is applied in the streamwise direction. In this case the compressibility effect becomes negligible and only the rarefaction effect is accounted for. Since a periodic channel can be regarded as an infinitely long channel, Eq. (4.3) is also valid for the prediction of slip velocity in a periodic channel under an external pressure gradient. Two different channel heights are considered to examine grid effects: $H=50\delta x$ and $100\delta x$. The external pressure gradient is implemented by setting $F_x=-\partial P/\partial x$ in Eq. (2.7). The slip velocity computed from the LBE simulation is obtained using the following formula:

$$U(y) = 4U_c\left(\frac{y}{H}-\frac{y^2}{H^2}\right)+U_s, \tag{4.4}$$

where the centerline velocity U_c and the slip velocity U_s are calculated by least squares fitting the numerical results. The slip velocity U_s is normalized to the centerline velocity.

Figure 1 compares the computed slip velocity U_s normalized to the centerline velocity U_c with Eq. (4.3). The normalized slip velocity is in excellent agreement with the analytical prediction in the regime below $\mathrm{Kn}<0.1$, although the computed slip velocity starts to deviate from the analytical result at higher Kn. Generally, the slip boundary condition used in [14] does not hold in the transition flow regime ($0.1<\mathrm{Kn}<3$). The results obtained from different H are vir-

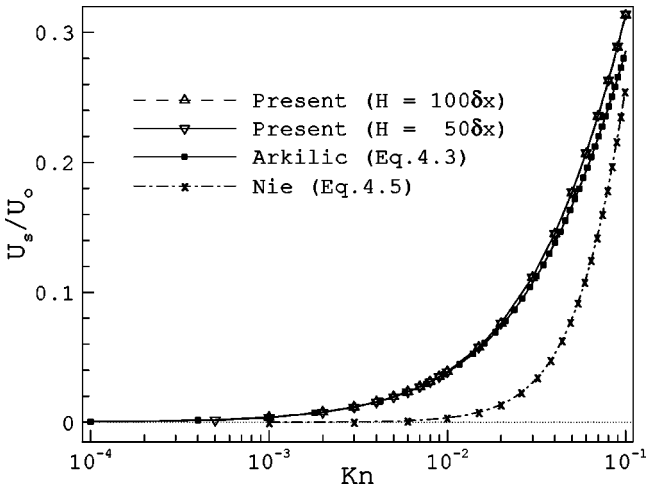

FIG. 1. Slip velocity in a periodic channel as a function of Kn. Flow is driven by external pressure gradient.

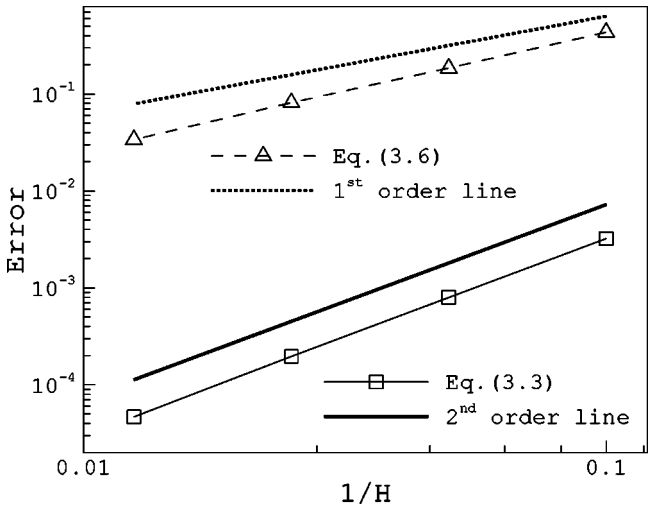

FIG. 2. Grid convergence of the normalized slip velocity.

tually identical. The dependence of the slip velocity on the Kn suggested by Nie *et al.* [8] is also shown in Fig. 1. In terms of the definition of the slip velocity given in Eq. (4.4), the normalized slip velocity of Nie *et al.* in the periodic channel can be written as (see Appendix B)

$$\frac{U_s}{U_c} = \frac{8.7\mathrm{Kn}^2}{0.25 + 8.7\mathrm{Kn}^2}, \tag{4.5}$$

in which the coefficient 8.7 is calculated to fit their numerical results. As will be discussed later, the Kn of Nie *et al.* requires a tunable parameter that must be chosen to best match the simulated mass flow rate with experiments and may not be dimensionless. In Fig. 1, their normalized slip velocity increases more rapidly at higher Kn than Arkilic's formula due to quadratic dependence of the slip velocity on Kn in Eq. (4.5), although less degree of slip is observed at lower Kn. This is because the bounce-back boundary condition adopted by Nie *et al.* is expected to allow less degree of slip at a given Kn. In the bounce-back scheme, when a particle distribution function streams to a wall node, the particle distribution function scatters back to the node it comes from. Collision does not occur on the solid boundaries.

Grid convergence of the present LBE method is shown in Fig. 2. Kn is fixed at 0.1 and calculations are performed on four systematically refined grids ($H = 10\delta x, 20\delta x, 40\delta x, 80\delta x$). The relative error to the fine grid result is measured by

$$(\text{error}) = \left| \frac{U_{s,o}/U_o(H) - U_{s,o}/U_o(H_{\text{fine}})}{U_{s,o}/U_o(H_{\text{fine}})} \right|, \tag{4.6}$$

where $H_{\text{fine}} = 320\delta x$. As is shown in the figure, the second-order spatial accuracy of the scheme is verified for the present definition of Kn, i.e., Eq. (3.2). The τ-Kn relation Eq. (3.6) of Lim *et al.* is also tested. Figure 2 shows that Eq. (3.6) gives only slightly better results than first-order accurate solutions.

The error of the solution based on the profile of the streamwise velocity $u(y)$ is examined as well. In order to demonstrate spatial accuracy, calculations are performed on three systematically refined grids (denoted by the subscripts $4h$ for $H = 20\delta x$, $2h$ for $H = 40\delta x$, and h for $H = 80\delta x$). Since the ratio of the grid spacing on successive grids is 2, the order of the scheme, p, can be estimated from [24]

$$p = \frac{\ln[(u_{2h} - u_{4h})/(u_h - u_{2h})]}{\ln 2}, \tag{4.7}$$

which yields $p = 2$ for Eq. (3.2). This confirms the second-order accuracy of the definition of Kn as well as the boundary condition.

Validation of the wall equilibrium boundary condition and the definition of Kn proposed in the previous section is performed by comparing the LBE results with those of the linearized Boltzmann equation [25] and the direct simulation Monte Carlo methods [22] for Kn = 0.1. For this purpose, the streamwise velocity profile $U(y)$ is normalized to the local averaged velocity $\overline{U}$. Analytical prediction due to the first-order slip condition can be made by considering the local volumetric flow rate and takes the form of

$$U^*(y) \equiv \frac{U(y)}{\overline{U}} = \frac{(y/H - y^2/H^2 + \sigma\mathrm{Kn})}{1/6 + \sigma\mathrm{Kn}}. \tag{4.8}$$

In Fig. 3(a), the velocity profiles obtained by the LBE, both first- and second-order slip conditions [22], the linearized Boltzmann equation, and the DSMC method are displayed for comparison. The error in Fig. 3(b) is measured by the deviation from the solution of the linearized Boltzmann equation, i.e., $(\text{error}) = U^* - U^*_{\text{lin Boltzmann}}$. The assumption made in the linearized Boltzmann simulation is that the gas molecules are reflected diffusely on the boundary, and the DSMC simulations are carried out for a nominal value of $\sigma_v = 1$. In general, the LBE solution is in excellent agreement with others. The error of the LBE solution is smallest around the centerline of the microchannel and increases near the boundaries.

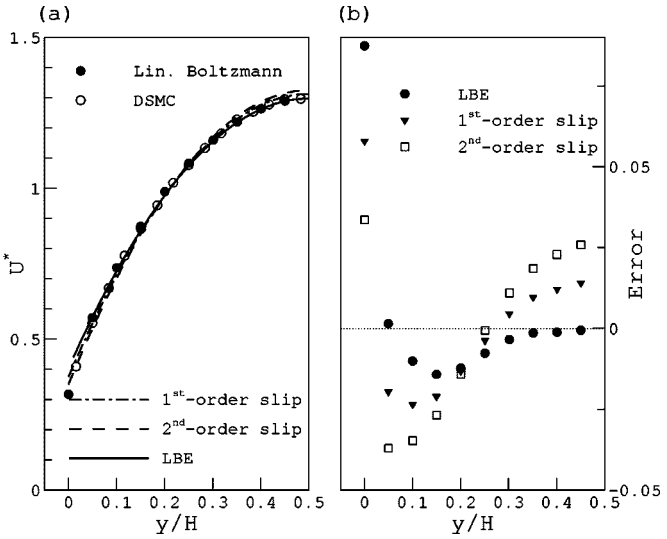

FIG. 3. (a) Nondimensional velocity distribution in half of a microchannel. The linearized Boltzmann solution is from Ohwada *et al.* [25] and the DSMC solution is from Karniadakis and Beskok [22]. (b) Deviations from the linearized Boltzmann solution.

The wall equilibrium boundary condition is further validated for the solution of the Kramers' problem, where the analytic solution of the continuous Boltzmann equation is available. The Kramers' problem is a plane Couette flow in which the distance of the walls H tends to infinity, while the speed U_∞ of the upper wall also goes to infinity with H such that the shear rate $k=U_\infty/H$ remains finite. The analytic solution for the macroscopic slip velocity U_s can be obtained in closed form and is given by $U_s=(1.016\,15)kl$ [26], l being the mean free path. Figure 4 compares the computed normalized macroscopic slip velocities with the analytic solution. As above, periodic boundary condition is applied in the streamwise direction and two different channel heights are considered to examine grid effects: $H=50\delta x$ and $100\delta x$. The shear rate is fixed at $k=0.001$ for both cases. The normalized slip velocities U_s/U_∞ are calculated by least squares fitting the numerical results. The normalized slip velocities are in excellent agreement with the analytical solution in the regime below $\mathrm{Kn}<0.1$.

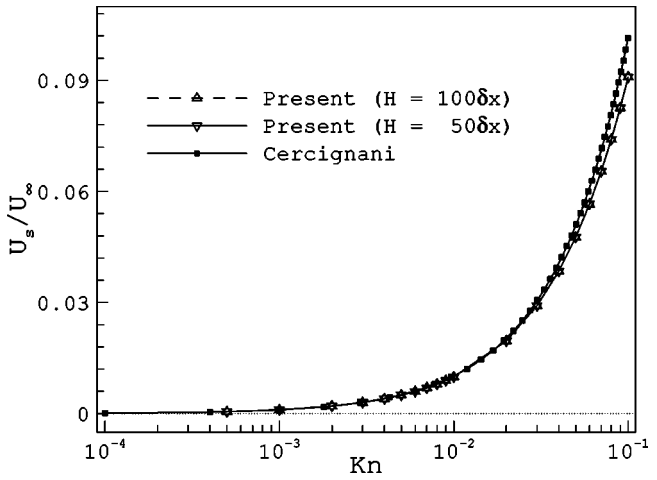

FIG. 4. Normalized macroscopic slip velocity at the stationary wall in the simulation of Kramers' problem. Shear rate $k=U_\infty/H=0.001$ and slip velocity $U_s=(1.016\,15)kl$ [26].

B. Gas flows in a long microchannel with pressure boundary condition

We now consider a long microchannel case with prescribed pressure boundary conditions at both inlet and outlet, which is commonly found in practical applications. Due to the rarefaction and compressibility effects, the pressure distribution along the microchannel is nonlinear. The pressure distribution along the channel predicted from the above first-order slip boundary condition is given by [14]

$$P/P_o = -6\sigma \mathrm{Kn}_o + \sqrt{(-6\sigma \mathrm{Kn}_o)^2 + (1+12\sigma \mathrm{Kn}_o)x/L + (\mathcal{P}^2 + 12\sigma \mathrm{Kn}_o \mathcal{P})(1-x/L)}, \tag{4.9}$$

where the inlet-to-outlet-pressure ratio is $\mathcal{P}=P_i/P_o$. Figure 5 shows the normalized slip velocity and nonlinearity of pressure along the microchannel at $\mathcal{P}=2.0$ with $H=50\delta x$. Wall boundaries are located halfway between two grid points for second-order accuracy [8]. The slip velocity U_s is obtained in the same way as in the periodic channel case and is normalized to the outlet centerline velocity U_o. The pressure deviation from the linear distribution $(P-P_{\mathrm{incomp}})$ is normalized to the outlet pressure P_o. L/H is taken inversely proportional to Kn_o such that the reference velocity of the system is kept constant. The reader is reminded that the LBE is second-order accurate in Mach number as well as time and space. We take the reference velocity as the centerline velocity of the incompressible flow without rarefaction effect, which can be written as

$$U_R = -\frac{H^2}{8\mu}\frac{P_o - P_i}{L}. \tag{4.10}$$

The reference velocity is fixed at $U_R=0.0625$ for all the test cases in the present section.

In Fig. 5, the compressibility effect results in the negative curvature of pressure distribution, while the rarefaction effect reduces it [7]. Figure 5 also indicates that the rarefaction effect of the LBE simulation increases slightly faster than the analytical solutions of Arkilic *et al.* [14] and the nonlinearity of the pressure is weaker at high Kn_o. Lim *et al.* [10] ob-

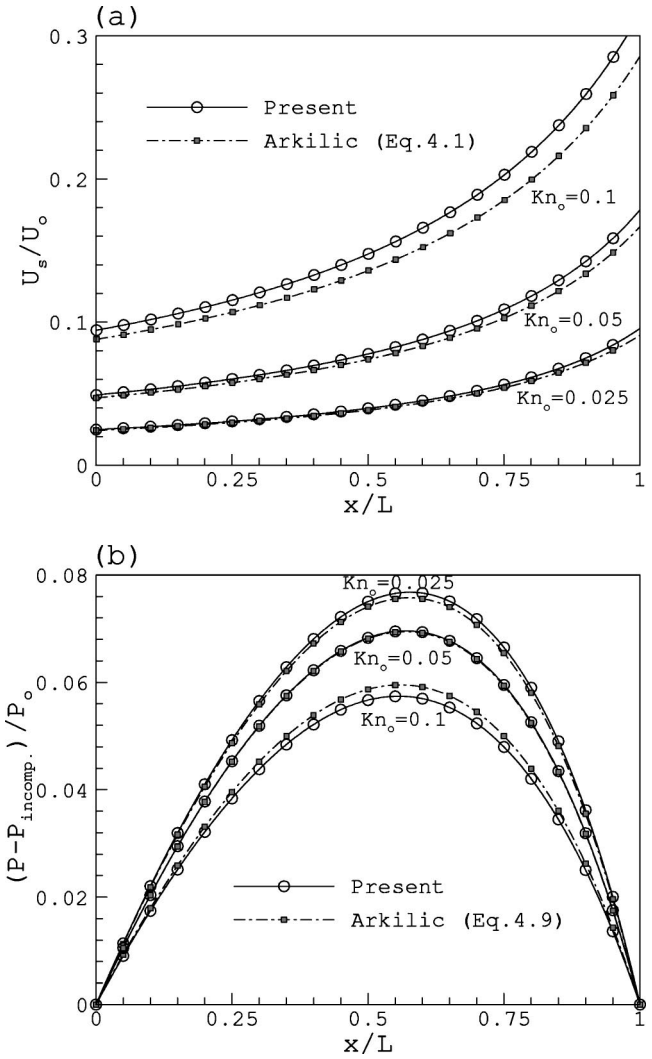

FIG. 5. Comparison of slip velocity and nonlinearity of pressure at $\mathcal{P}=2.0$, $H=50$. $L/H=20$, 40, and 80 for $\mathrm{Kn}_o=0.1$, 0.05, and 0.025, respectively. (a) Slip velocity normalized to the outlet centerline velocity, and (b) deviation of the pressure from the linear pressure distribution normalized to the outlet pressure.

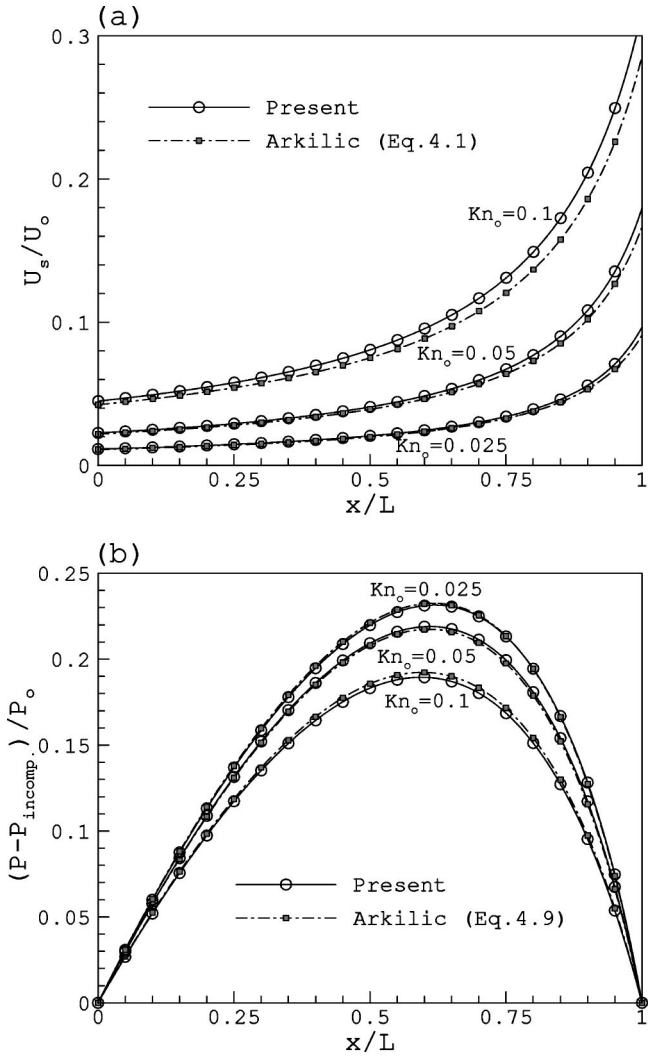

FIG. 6. Comparison of slip velocity and nonlinearity of pressure at $\mathcal{P}=3.0$, $H=50$. $L/H=40$, 80, and 160 for $\mathrm{Kn}_o=0.1$, 0.05, and 0.025, respectively. (a) Slip velocity normalized to the outlet centerline velocity, and (b) deviation of the pressure from the linear pressure distribution normalized to the outlet pressure.

served a similar trend in the rarefaction effect. Figure 6 shows the results at $\mathcal{P}=3.0$ with $H=50\delta x$. The outlet slip velocity at $\mathcal{P}=3.0$ is virtually identical to that at $\mathcal{P}=2.0$, since it follows from Eq. (4.3) that the outlet slip velocity is only a function of Kn_o. This observation is consistent with the slip velocity computed in a periodic microchannel in Fig. 5. The deviation from the analytical solution at higher $\mathcal{P}$ is smaller as compared with Fig. 5. The nonlinearity of the pressure due to the enhanced compressibility effect is much more evident at higher pressure ratio and the curvature of the slip velocity along the channel increases accordingly.

In Fig. 7, the slip velocity and the pressure nonlinearity at $\mathrm{Kn}_o=0.05$ are compared with those of Lim *et al.* [10]. Two types of boundary conditions were used in their work. The first one is the specular boundary condition ("Spec." in the figure), which is analogous to a reflection of a particle hitting a wall specularly. The other is an extrapolation scheme ("U Ext." in the figure), which approximates the density and the streamwise velocity at solid boundaries by a second-order extrapolation scheme, and the unknown distribution functions at the wall are approximated by their equilibrium functions. Figure 7 shows that the slip velocity obtained by Lim *et al.* is generally much lower than both Arkilic *et al.*'s and the present results. In addition the predicted peak of the nonlinearity is more severely skewed toward the outlet. Lim *et al.* argued that mere incorporation of a first-order slip boundary condition in the Navier-Stokes equations would not sufficiently and accurately account for the slip phenomenon. The derivation of the analytical formula is based upon the assumptions that the pressure across the channel is constant and the effect of the inertial term is negligible, which may become invalid as Kn_o increases. The presence of the inertial term generally enhances the slip velocity and reduces the pressure nonlinearity. It is expected that the effect of the inertial term would become more evident with increasing slip velocity and Kn_o as well.

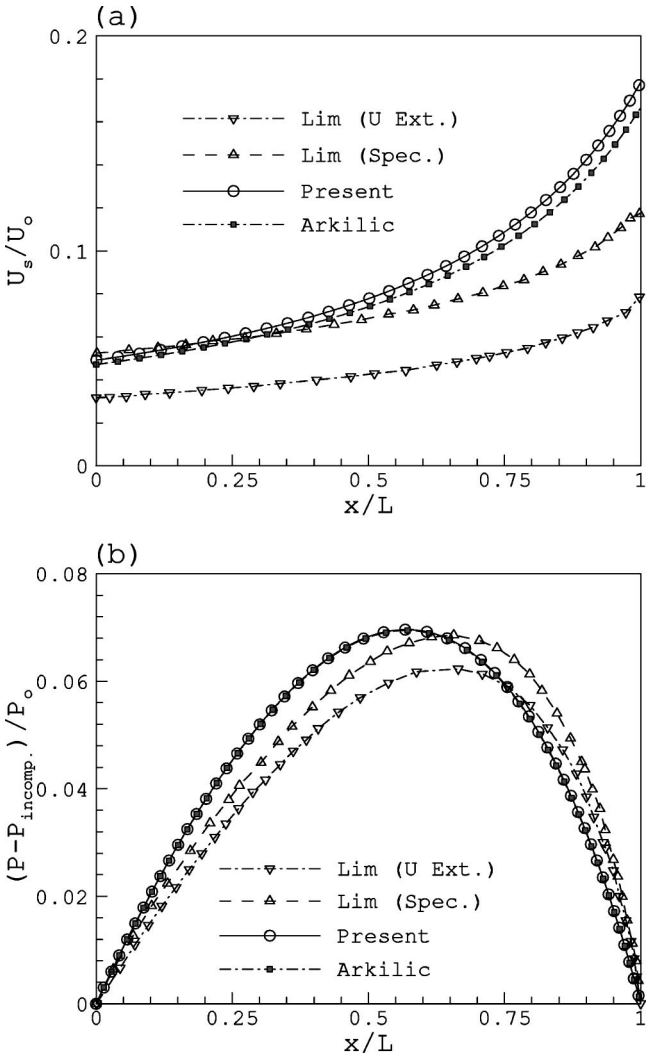

FIG. 7. Comparison of slip velocity and nonlinearity of pressure with those in Lim *et al.* [10] $\mathrm{Kn}_o=0.05$ and $\mathcal{P}=2.0$.

Even though only the rarefaction effect is accounted for in Arkilic *et al.*'s solution by incorporating a first-order slip, our results are in excellent agreement with the analytical formula. The disagreement between the analytical formula and the previous LBE results by others may be attributed to the definition of Kn and the boundary conditions. By introducing the proper Kn and the wall equilibrium boundary condition, the LBE method can deal with gas flows in the higher-Kn regime as well as in the slip flow regime. Various definitions of Kn, boundary conditions, and numbers of grid used in the previous computations as well as the present work are summarized in Table I. The Kn of Nie *et al.* requires a tunable parameter α that must be chosen to best match the simulated mass flow rate with experiments. In the case that α is a dimensionless parameter, Kn is no longer a dimensionless number. The Kn of Lim *et al.* is only first-order accurate as shown above. Compared with the wall equilibrium boundary condition that assumes diffuse reflection, the bounce-back boundary condition used by Nie *et al.* is expected to allow less degree of slip at a given Kn. In the bounce-back scheme, when a particle distribution function streams to a wall node, the particle distribution function scatters back to the node it comes from. Collision does not occur on the solid boundaries. As can be seen in Fig. 1, the normalized slip velocity obtained from the bounce-back boundary condition of Nie *et al.* is much lower than the analytical formula and that from the wall equilibrium boundary condition. The specular bounce-back boundary condition used by Lim *et al.* supposedly allows more slip effect, although their specular bounce-back scheme is not perfectly specular. Collision occurs on the solid boundaries and the distribution functions parallel to the solid boundaries are calculated by LBE. Therefore, their specular model still has some momentum deposited on the wall and only the unknown distribution functions are defined by their corresponding specular directions [10]. By comparison, the perfect specular slip boundary condition used by Succi [11] does not consider collision on the solid boundaries. Consequently, the specular bounce-back scheme of Lim *et al.* still results in weaker slip effect than the analytical formula and the wall equilibrium boundary condition as in Fig. 7. The extrapolation scheme has less physical ground, but Lim *et al.* used it to investigate the direct effects of boundary treatments on slip velocity.

The effect of rarefaction on mass flow rate is investigated by comparison of the LBE result with experimental data as well as analytical predictions. The nondimensional mass flow rate M^* can be expressed as a function of pressure ratio (see Appendix A)

$$M^* = \frac{\dot{M}}{\dot{M}_{\text{no slip}}} = 1 + 12\sigma\frac{\mathrm{Kn}_o}{\mathcal{P}+1}. \tag{4.11}$$

In Fig. 8, the nondimensional mass flow rate computed by the LBE method for $U_R=0.0625$ is compared with the first-order analytical prediction Eq. (4.11) and the experimental data of Arkilic *et al.* [14]. In their experiments, Arkilic *et al.* investigated helium gas flow having $\mathrm{Kn}_o=0.165$. For all cases, slip effects become less pronounced with increasing pressure ratio. Equation (4.11) deviates from the experiments especially at low pressure ratios. The LBE results generally

TABLE I. Comparison of computational conditions in the literature.

	Kn[a]	Boundary condition	Channel height $H(\delta x)$
Nie *et al.* [8]	$\mathrm{Kn}=\alpha\tau/\rho H$[b]	Bounce back	$10\delta x$
Lim *et al.* [10]	$\mathrm{Kn}=\delta x(\tau+0.5)/H(P_o/P)$	Specular bounce back and extrapolation	$10\delta x-20\delta x$
Present work	$\mathrm{Kn}=\delta x\tau/H(P_o/P)$	Wall equilibrium	$10\delta x-320\delta x$

[a] τ defined in Eq. (2.7).
[b] α is chosen to best match the simulated mass flow rate with experiments.

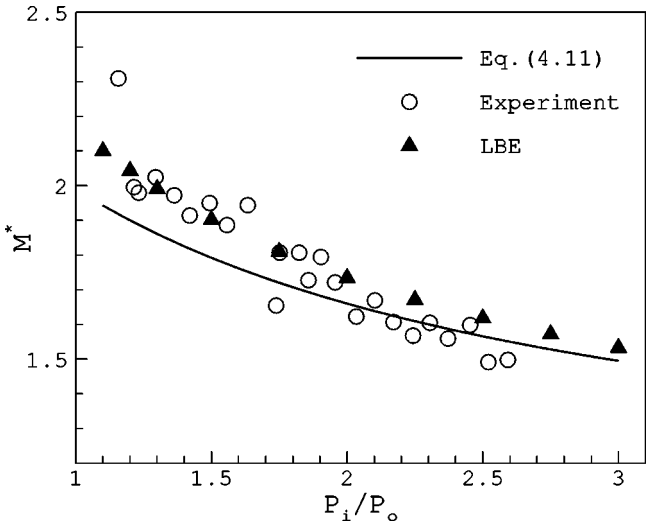

FIG. 8. Mass flow rate normalized to no-slip mass flow rate as a function of pressure ratio at $\mathrm{Kn}_o=0.165$. The experimental data are from Arkilic *et al.* [14].

agree well with the experiments and show slightly more mass flow rate at high pressure ratios.

V. CONCLUDING REMARKS

In the paper, we demonstrate that the LBE simulation of gas flows in a microchannel can be successful if the proper definition of Kn and the wall equilibrium boundary condition are applied. Second-order spatial accuracy of the LBE method in the microchannel application is verified. In the slip flow regime, the computed slip velocity and the pressure nonlinearity are in excellent agreement with the analytical formula by Arkilic *et al.* [14]. As the size of the microfluidic devices becomes smaller, the transition flow regime ($0.1<\mathrm{Kn}<10$) draws more attention. In this intermediate-to-high-Kn flow, *virtual wall collisions* proposed by Toschi and Succi [27] can be a promising approach.

Future research areas may include investigation of the boundary condition for the case of the nonzero tangential momentum accommodation coefficient [11]. Thermal effects [28] and irregular geometries [9] are other examples of urgent research directions of the LBE method in microsystems.

ACKNOWLEDGMENTS

This work was supported by the Carver Scientific Research Initiative Grants Program at the University of Iowa. The partial support of the IIHR Hydroscience & Engineering at the University of Iowa is also acknowledged.

APPENDIX A

The streamwise velocity profile with rarefaction effect is given by Arkilic *et al.* [14]:

$$U(x,y) = -\frac{H^2}{2\mu}\frac{dP}{dx}\left(\frac{y}{H}-\frac{y^2}{H^2}+\sigma\mathrm{Kn}\right), \tag{A1}$$

whose coordinate system is located at the bottom of the inlet. The streamwise velocity profile normalized to the centerline velocity at the outlet (U_o) is

$$\frac{U(x,y)}{U_o} = \frac{dP/dx}{dP_o/dx}\frac{(y/H-y^2/H^2+\sigma\mathrm{Kn})}{(0.25+\sigma\mathrm{Kn}_o)}. \tag{A2}$$

The mass flow rate corresponding to Eq. (A1) is computed by multiplying Eq. (A1) by the density and integrating across the channel. The dimensional mass flow rate is given by

$$\dot{M} = \frac{H^3P_o^2}{24\mu RTL}[(\mathcal{P}^2-1)+12\sigma\mathrm{Kn}_o(\mathcal{P}-1)], \tag{A3}$$

where $\mathcal{P}\equiv P_i/P_o$. The mass flow rate without the rarefaction effects is

$$\dot{M}_{\text{no slip}} = \frac{H^3P_o^2}{24\mu RTL}(\mathcal{P}^2-1). \tag{A4}$$

APPENDIX B

The definition of the slip velocity in Nie *et al.* [8] originally takes the form

$$U(y) = V_o\left(\frac{y}{H}-\frac{y^2}{H^2}+V_s\right), \tag{B1}$$

whose coordinate system is located at the bottom of the inlet. They fitted the data by the least squares method to get $V_s=8.7\mathrm{Kn}_o^2$, which leads to Eq. (4.5), if $U_s\equiv V_oV_s$ is normalized to the outlet centerline velocity $V_o(0.25+V_s)$.

[1] Q. Zou and X. He, Phys. Fluids **9**, 1591 (1997).
[2] R. Benzi, S. Succi, and M. Vergassola, Phys. Rep. **222**, 145 (1992).
[3] S. Chen and G. D. Doolen, Annu. Rev. Fluid Mech. **30**, 329 (1998).
[4] Y. Zohar, S. Y. K. Lee, W. Y. Lee, L. Jiang, and P. Tong, J. Fluid Mech. **472**, 125 (2002).
[5] K. C. Pong, C. M. Ho, J. Q. Liu, and Y. C. Tai, FED (Am. Soc. Mech. Eng.) **197**, 51 (1994).
[6] E. S. Oran, C. K. Oh, and B. Z. Cybyk, Annu. Rev. Fluid Mech. **30**, 403 (1998).
[7] A. Beskok, G. E. Karniadakis, and W. Trimmer, J. Fluids Eng. **118**, 448 (1996).
[8] X. Nie, G. D. Doolen, and S. Chen, J. Stat. Phys. **107**, 279 (2002).
[9] T. Lee and C.-L. Lin, J. Comput. Phys. **185**, 445 (2003).
[10] C. Y. Lim, C. Shu, X. D. Niu, and Y. T. Chew, Phys. Fluids **14**, 2299 (2002).

[11] S. Succi, Phys. Rev. Lett. **89**, 064502 (2003).
[12] X. Y. He, Q. S. Zou, L. S. Luo, and M. Dembo, J. Stat. Phys. **87**, 115 (1997).
[13] S. Ansumali and I. V. Karlin, Phys. Rev. E **66**, 026311 (2002).
[14] E. B. Arkilic, M. A. Schmidt, and K. S. Breuer, J. Microelectromech. Syst. **6**, 167 (1997).
[15] X. He, S. Chen, and G. D. Doolen, J. Comput. Phys. **146**, 282 (1998).
[16] T. Inamuro, M. Yoshino, and F. Ogino, Phys. Fluids **9**, 3535 (1997).
[17] Y.-H. Qian and S.-Y. Chen, Phys. Rev. E **61**, 2712 (2000).
[18] X. He, X. Shan, and G. D. Doolen, Phys. Rev. E **57**, R13 (1998).
[19] L. B. Loeb, *The Kinetic Theory of Gases* (McGraw-Hill Book Company, New York, 1934).
[20] E. B. Arkilic, K. S. Breuer, and M. A. Schmidt, FED (Am. Soc. Mech. Eng.) **197**, 57 (1994).
[21] S. A. Schaaf and P. L. Chambré, *Flow of Rarefied Gases* (Princeton University Press, Princeton, NJ, 1961), pp. 10–11.
[22] G. E. Karniadakis and A. Beskok, *Micro Flows* (Springer, Berlin, 2000).
[23] S. Chen, D. Martínez, and R. Mei, Phys. Fluids **8**, 2527 (1996).
[24] J. H. Ferziger and M. Perić, *Computational Methods for Fluid Dynamics* (Springer, Berlin, 2002).
[25] T. Ohwada, Y. Sone, and K. Aoki, Phys. Fluids A **1**, 2042 (1989).
[26] C. Cercignani, *Rarefied Gas Dynamics* (Cambridge University Press, Cambridge, U.K., 2000).
[27] F. Toschi and S. Succi, Europhys. Lett. **69**, 549 (2005).
[28] Y. Zheng, A. Garcia, and B. Alder, J. Stat. Phys. **109**, 495 (2002).